# X-ray Absorption Spectroscopy of Calcium-Substituted Derivatives of the Oxygen-Evolving Complex of Phostosytem II

**Pamela J. Riggs-Gelasco,[†] Rui Mei,[‡,§] Demetrios F. Ghanotakis,[⊥] Charles F. Yocum,*[,†,‡] and James E. Penner-Hahn*[,†]**

*Contribution from the Departments of Chemistry and Biology, University of Michigan, Ann Arbor, Michigan 48109, and Chemistry Department, University of Crete, Iraklion, Crete, Greece*

*Received February 9, 1995. Revised Manuscript Received June 12, 1995*[⊗]

**Abstract:** X-ray absorption spectroscopy (XAS) has been used to characterize the structural consequences of $Ca^{2+}$ replacement in the reaction center complex of the photosynthetic oxygen-evolving complex (OEC). EPR and activity measurements demonstrate that, in the absence of the 17 and 23 kDa extrinsic polypeptides, it is not necessary to use either low pH or Ca chelators to effect complete replacement of the active site $Ca^{2+}$ by $Sr^{2+}$, $Dy^{3+}$, or $La^{3+}$. The extended X-ray absorption fine structure (EXAFS) spectra for the OEC show evidence for a Mn···M interaction at ca. 3.3 Å that could arise either from Mn···Mn scattering within the Mn cluster or Mn···Ca scattering between the Mn cluster and the inorganic $Ca^{2+}$ cofactor. There is no significant change in the either the amplitude or the phase of this feature when $Ca^{2+}$ is replaced by $Sr^{2+}$ or $Dy^{3+}$, thus demonstrating that there is no EXAFS-detectable Mn···Ca contribution at ca. 3.3 Å in these samples. The only significant consequence of $Ca^{2+}$ replacement is a small change in the ca. 2.7 Å Mn···Mn distance. The average Mn···Mn distance decreases 0.014 Å when $Ca^{2+}$ is replaced by $Sr^{2+}$ and increases 0.012 Å when $Ca^{2+}$ is replaced by $Dy^{3+}$. A structural model which can account both for the variation in Mn···Mn distance and for the known properties of $Ca^{2+}$-substituted samples is one in which there is a hydrogen bond between a $Ca^{2+}$-bound water and a $Mn_2(\mu\text{-}O)_2$ unit. This scheme suggests that an important role for the $Ca^{2+}$ may be to modulate the protonation state, and thus the redox potential, of the Mn cluster.

The oxidation of $H_2O$ during photosynthesis is accomplished by the Oxygen-Evolving Complex (OEC)[1] of Photosystem II (PSII). The redox activity of the enzyme arises from the sequential accumulation of four oxidizing equivalents that are ultimately utilized to oxidize two $H_2O$ molecules to $O_2$.[2] Kok[3] described the redox intermediates as $S_i$ states, $i = 0-4$. The Mn cluster in the OEC is believed to contain 4 Mn atoms bound in the +3 and +4 oxidation states.[4−6] The Mn cluster is oxidized on the $S_0 \rightarrow S_1$, $S_1 \rightarrow S_2$, and possibly $S_2 \rightarrow S_3$ transitions, establishing that the Mn cluster is critical for catalytic activity.[3,7−9] In addition, $Ca^{2+}$ and $Cl^-$ are required for activity.[10,11] The requirement for Mn is stringent, whereas $Ca^{2+}$ can be replaced by $Sr^{2+}$ and $Cl^-$ can be replaced by $Br^-$.

The role of $Ca^{2+}$ in the OEC is not clearly understood. In the absence of the 23- and 17-kDa extrinsic polypeptides, nonphysiological concentrations of both $Ca^{2+}$ and $Cl^-$ are required for maximal activity.[12−14] If these polypeptides are reconstituted in the absence of $Ca^{2+}$, incubation with $Ca^{2+}$ for up to an hour is necessary to reestablish activity, suggesting that the 17- and 23-kDa proteins may block access of $Ca^{2+}$ to its active site.[15,16] Most studies suggest that there are two distinct binding sites present in higher plants.[16−19] A low-affinity $Ca^{2+}$ site has a $K_m \approx 1-2$ mM, whereas a more tightly bound calcium has a $K_m \approx 50-100$ $\mu$M.[20,21] A recent study, however, suggests that there may be three binding sites, with $K_m$ values of 1−4 $\mu$M, 67−97 $\mu$M, and 2.7−7 mM.[21]

Initial studies of the importance of $Ca^{2+}$ in $H_2O$ oxidation focused on its replacement by other metals. The lanthanides

[†] Department of Chemistry, University of Michigan.
[‡] Department of Biology, University of Michigan.
[§] Current address: Department of Biochemistry, Stanford University, Beckman Center, Stanford, CA 94305.
[⊥] Chemistry Department, University of Crete.
[⊗] Abstract published in *Advance ACS Abstracts,* February 1, 1996.

(1) Abbreviations used: chl = chlorophyll; EDTA = ethylenedamine-tetraacetic acid; EGTA = ethyleneglycol bis($\beta$-aminoethyl ether)-*N*,*N*,*N*′,*N*′-tetracetate; EPR = electron paramagnetic resonance; EXAFS = Extended X-ray Absorption Fine Structure; kDa = kilodalton; Ln = any lanthanide; MES = 2-(*N*-morpholino)ethanesulfonic acid; OEC = Oxygen Evolving Complex; PSII = Photosystem II; salpn=1,3-bis(salicylideneiminato)-propane; XANES = X-ray Absorption Near Edge Structure; XAS = X-ray Absorption Spectroscopy.

(2) Joliet, P.; Barbierri, G.; Chabaud, R. *Photochem. Photobiol.* **1969**, *10*, 309−329.
(3) Kok, B.; Forbush, B.; McGloin, M. *Photochem. Photobiol.* **1970**, *11*, 457.
(4) Sivaraja, M.; Dismukes, G. C. *Biochemistry* **1988**, *27*, 3467−3475.
(5) Cheniae, G.; Martin, I. *Biochim. Biophys. Acta* **1970**, *197*, 219−239.
(6) Yocum, C. F.; Yerkes, C. T.; Blankenship, R. E.; Sharp, R. R.; Babcock, G. T. *Proc. Natl. Acad. Sci. U.S.A.* **1981**, *78*, 7507−7511.
(7) Ono, T.-a.; Noguchi, T.; Inoue, Y.; Kusunoki, M.; Matsushita, T.; Oyanagi, H. *Science* **1992**, *258*, 1335−1337.
(8) Guiles, R. D.; J.-L., Z.; McDermott, A. E.; Yachandra, V. K.; Cole, J. L.; Dexheimer, S. L.; Britt, R. D.; Wieghardt, K.; Bossek, U.; Sauer, K.; Klein, M. P. *Biochemistry* **1990**, *29*, 471−485.
(9) Yachandra, V. K.; Guiles, R. D.; McDermott, A. E.; Cole, J. L.; Britt, R. D.; Dexheimer, S. L.; Sauer, K.; Klein, M. P. *Biochemistry* **1987**, *26*, 5974−5981.
(10) Yocum, C. F. *Biochim. Biophys. Acta* **1991**, *1059*, 1−15.
(11) Debus, R. J. *Biochim. Biophys. Acta* **1992**, *1102*, 269−352.
(12) Ghanotakis, D. F.; Babcock, G. T.; Yocum, C. F. *FEBS Lett.* **1985**, *192*, 1−3.
(13) Ghanotakis, D. F.; Babcock, G. T.; Yocum, C. F. *FEBS Lett.* **1984**, *167*, 127−130.
(14) Miyao, M.; Murata, N. *FEBS Lett.* **1984**, *168*, 118−120.
(15) Ghanotakis, D. F.; Topper, J. N.; Babcock, G. T.; Yocum, C. F. *FEBS Lett.* **1984**, *170*, 169.
(16) Ono, T.-A.; Yorinao, I. *FEBS Lett.* **1988**, *227*, 147−152.
(17) Boussac, A.; Rutherford, A. W. *Biochemistry* **1988**, *27*, 3476−3483.
(18) Homann, P. H. *Biochim. Biophys. Acta* **1988**, *934*, 1−13.
(19) Shen, J.-R.; Satoh, K.; Katoh, S. *Biochim. Biophys. Acta* **1988**, *933*, 358−364.
(20) Cammarata, K. V.; Cheniae, G. M. *Plant Physiol.* **1987**, *84*, 587−589.
(21) Kalosaka, K.; Beck, W. F.; Brudvig, G.; Cheniae, G. *Curr. Res. Photosynth.* **1990**, *1*, 721−724.

0002-7863/96/1518-2400$12.00/0 

($Ln^{3+}$) are very effective competitive inhibitors of the $Ca^{2+}$ site, despite the increased charge on $Ln^{3+}$. The $K_i$ for $La^{3+}$ was estimated to be 0.05 mM compared to the $K_m$ for $Ca^{2+}$ of 0.5 mM.[22] In the initial studies, it was found that both Mn and the extrinsic polypeptides (17, 23, and 33 kDa) were released on addition of $Ln^{3+}$.[22] However, recent work has shown that the 33-kDa polypeptide and Mn can be retained if high concentrations of NaCl are present during exposure to lanthanides.[23] $Cd^{2+}$ has relatively high affinity for the $Ca^{2+}$ site(s), showing mixed-competitive inhibition with a $K_i$ of 0.3 mM.[24] Monovalent cations ($Na^+$, $K^+$, and $Cs^+$) weakly inhibit calcium activation of oxygen evolution ($K_i \approx 8$ mM[24]). Finally, $Mn^{2+}$ itself can compete for the calcium binding site(s) in photoactivation and in cation reconstitution studies.[13,25,26]

In addition to studies of $Ca^{2+}$ replacement, there have been numerous investigations of $Ca^{2+}$-depleted PSII. One difficulty with these studies is that the actual extent of $Ca^{2+}$ depletion in PSII is difficult to assess. Most studies employ combinations of NaCl and chelators (EGTA,[27,28] EDTA, or chelex[19]), illumination, lowered pH,[16] or the ionophore A23187[20] for $Ca^{2+}$ removal. These treatments impair oxygen evolution, most likely by removing $Ca^{2+}$ from the lower affinity site(s). It is now generally accepted that extremely stringent conditions must be employed for complete $Ca^{2+}$ removal. Harsher treatments remove a tightly bound calcium of unknown function. One such treatment is lanthanide substitution, which is reported to effectively remove all calcium.[23]

The affinity of $Ca^{2+}$ for its site(s) is thought to depend on both the redox state of the Mn cluster and the presence of extrinsic polypeptides. In the absence of the 23-kDa polypeptide, the $Ca^{2+}$ responsible for OEC activation has a low affinity for its binding site and can be readily replaced by competing cations.[14,15,29] The binding affinity of calcium is highest in $S_1$ and weakest in $S_3$,[28] a finding consistent with the observation that illumination facilitates removal of $Ca^{2+}$ in the presence of chelators.[29,30]

In addition to blocking activity, $Ca^{2+}$ depletion also affects the EPR properties of the $S_2$ state.[27,31] The multiline EPR signal in the native $S_2$ state is centered at $g \approx 2$, with 16−18 lines having ∼80-G spacings.[27] The multiline signal in $Ca^{2+}$-depleted samples has about 26 resolved lines with an average spacing of 55 G, and can be observed in samples where $Ca^{2+}$ was removed with chelators or by a low pH treatment.[31,32] The $S_2$ multiline signal associated with $Ca^{2+}$-depleted samples is unusual in that it is dark stable. Further illumination of samples exhibiting this altered multiline signal leads to formation of a 164 G wide, $g = 2$ signal that has been attributed to $S_3$.[27]

If the $Ca^{2+}$ site is occupied by $Sr^{2+}$, the multiline signal amplitude is diminished in favor of the $S_2$ $g \approx 4.1$ EPR signal.[28] The multiline signal can still be formed in the presence of $Sr^{2+}$, but in this case it is modified (decreased line spacing and redistributed splittings) relative to the native OEC.[28]

The effect of $Ca^{2+}$ depletion on the Mn multiline signal and the dependence of $Ca^{2+}$ affinity on S state suggest that the $Ca^{2+}$ site that is responsible for activation of $H_2O$ oxidation is near the Mn cluster. If so, it may be detectable by extended X-ray absorption fine structure (EXAFS) spectroscopy. There is general agreement that EXAFS spectra of the OEC show Mn···metal scattering peaks at approximately 2.7 and 3.3−3.6 Å.[33−36] The 2.7-Å interaction is attributed to Mn···Mn scattering from $Mn(\mu\text{-}O)_2Mn$ units. However, interpretation of the more distant interaction has proven more controversial.

The first suggestion that there might be scatterers at >3 Å was made by Klein, Sauer, and their co-workers,[37] although these workers subsequently showed that the original long distance feature was not reproducible.[8] Later work, using lower temperature measurements, showed reproducible features at $R$ > 3 Å, first in oriented[33] and subsequently in non-oriented samples.[38] Based on their polarization dependent measurements, George et al. attributed this feature to a Mn−Mn interaction at 3.3 Å.[33] Based on isotropic measurements, we have found that either Mn−Mn or Mn−Ca interactions can model the 3.3-Å feature and that there may be additional contributions from Mn−C scattering.[38] More recently, Nugent and co-workers have addressed this question, again using isotropic measurements. This group initially suggested that the distant scatterer was Ca, based on the fact that Mn−Ca interactions gave better fits than Mn−Mn interactions.[34] However, this group recently reported that Mn−Mn and Mn−Ca scattering can*not* be distinguished.[39] Recent work by Klein, Sauer, and their collaborators has indicated that Mn−Mn gives a better fit to the distant peak than does Mn−Ca.[35] Two-shell fits to the 3.3-Å feature were difficult to justify;[35,40] however, these authors have noted that this does not exclude the possibility that Ca or C also contributed to the 3.3-Å feature.[41,42]

In addition to uncertainty over the identity of the distant scatterers, there is even uncertainty over the Mn−metal distance. We,[36,38] together with George et al.[33] and the Klein/Sauer group,[35,41−43] have consistently found a Mn−metal distance of approximately 3.3 Å. In contrast, Nugent and co-workers have reported that the distance is 3.7 Å.[34,39]

These contradictory results illustrate the difficulty of fitting outer-shell EXAFS. Several factors contribute to the ambiguity in outer-shell scattering.[44,45] As distance from the Mn increases,

(22) Ghanotakis, D.; Babcock, G. T.; Yocum, C. F. *Biochim. Biophys. Acta* **1985**, *809*, 173−180.
(23) Bakou, A.; Buser, C.; Dandulakis, G.; Brudvig, G.; Ghanotakis, D. *Biochim. Biophys. Acta* **1992**, *1099*, 131−136.
(24) Waggoner, C. M. Ph.D. Thesis, University of Michigan, 1989.
(25) Ono, T.-A.; Inoue, Y. *Biochim. Biophys. Acta* **1983**, *723*, 191−201.
(26) Tamura, N.; Cheniae, G. M. *FEBS Lett.* **1986**, *200*, 231−236.
(27) Boussac, A.; Zimmerman, J.-L.; Rutherford, A. W. *Biochemistry* **1989**, *28*, 8984−8989.
(28) Boussac, A.; Rutherford, A. W. *FEBS Lett.* **1988**, *236*, 432−436.
(29) Boussac, A.; Maison-Peteri, B.; Etienne, A.-L.; Vernotte, C. *Biochim. Biophys. Acta* **1985**, *808*, 231−234.
(30) Miyao, M.; Murata, N. *Photosynth. Res.* **1986**, *10*, 489−496.
(31) Ono, T.-A.; Inoue, Y. *Biochim. Biophys. Acta* **1990**, *1015*, 373−377.
(32) Boussac, A.; Zimmerman, J.-L.; Rutherford, A. W. *FEBS Lett.* **1990**, *277*, 69−74.
(33) George, G. N.; Prince, R. C.; Cramer, S. P. *Science* **1989**, *243*, 789−791.
(34) MacLachlan, D. J.; Hallahan, B. J.; Ruffle, S. V.; Nugent, J. H. A.; Evans, M. C. W.; Strange, R. W.; Hasnain, S. S. *Biochem. J.* **1992**, *285*, 569−576.
(35) DeRose, V. J.; Mukerji, I.; Latimer, M. J.; Yachandra, V. K.; Sauer, K.; Klein, M. P. *J. Am. Chem. Soc.* **1994**, *116*, 5239−5249.
(36) Riggs-Gelasco, P.; Mei, R.; Yocum, C. F.; Penner-Hahn, J. E. *J. Am. Chem. Soc.* **1996**, *118*, 2387−2399.
(37) Guiles, R. D.; Yachandra, V. K.; McDermott, A. E.; Britt, R. D.; Dexheimer, S. L.; Sauer, K.; Klein, M. P. In *Progress in Photosynthesis Research*; Biggens, J., Ed.; Martinus Nijhoff Publishers: Dordrecht, The Netherlands, 1987; Vol. 1, pp 1.5.561−1.5.564.
(38) Penner-Hahn, J. E.; Fronko, R. H.; Pecoraro, V. L.; Yocum, C. F.; Betts, S. D.; Bowlby, N. R. *J. Am. Chem. Soc.* **1990**, *112*, 2549−2557.
(39) MacLachlan, D. J.; Nugent, J. H. A.; Bratt, P. J.; Evans, M. C. W. *Biochim. Biophys. Acta* **1994**, *1186*, 186−200.
(40) Dau, H.; Andrews, J. C.; Roelofs, T. A.; Latimer, M. J.; Liang, W.; Yachandra, V. K.; Sauer, K.; Klein, M. P. *Biochemistry* **1995**, *34*, 5274−5287.
(41) Liang, W.; Latimer, M. J.; Dau, H.; Roelofs, T. A.; Yachandra, V. K.; Sauer, K.; Klein, M. P. *Biochemistry* **1994**, *33*, 4923−4932.
(42) Mukerji, I.; Andrews, J. C.; DeRose, V. J.; Latimer, M. J.; Yachandra, V. K.; Sauer, K.; Klein, M. P. *Biochemistry* **1994**, *33*, 9712−9721.
(43) Yachandra, V. K.; DeRose, V. J.; Latimer, M. J.; Mukerji, I.; Sauer, K.; Klein, M. P. *Science* **1993**, *260*, 675−679.

the number of possible scatterers increases. For example, scattering from the carbons of coordinated amino acids could obscure a Mn···metal interaction. In addition, longer interactions often exhibit greater disorder and consequently their EXAFS oscillations can be strongly damped, making detection difficult. Finally, the two most likely scatterers to be found at this distance are Ca or Mn, and these elements have nearly indistinguishable backscattering properties.[45,46]

A more straightforward way to determine the identity of the 3.3-Å scatterer is to measure X-ray absorption spectra for $Ca^{2+}$-substituted samples. If the $Ca^{2+}$ is bound in the vicinity ($\leq$4 Å) of the Mn cluster, then changes in the EXAFS may be detected when the $Ca^{2+}$ is removed or when different metals replace the $Ca^{2+}$. On the basis of such an experiment, Yachandra et al. have recently assigned the 3.3-Å interaction to Mn···Ca scattering.[43,47,48] In this work, replacement of $Ca^{2+}$ by $Sr^{2+}$ substitution gave a significant increase in the amplitude of the third peak in the Fourier transform (i.e. the 3.3-Å interaction); a mixture of Sr and Mn produced the best fit for this interaction. Similarly, Nugent and co-workers have reported that outer-shell interaction (at 3.6 Å in their data) decreases in amplitude when $Ca^{2+}$ is replaced by $Na^{+}$. These results suggest that at least some of the outer-shell scattering is due to a Mn···Ca interaction. However, the results are not unambiguous. In the $Sr^{2+}$-substitution experiments, the noise level is relatively high and no curve-fitting results are given.[43,47,48] In the $Ca^{2+}$/$Na^{+}$ studies, the curve-fitting results show only a small change in the Debye−Waller factor for the putative Mn···Ca shell when $Ca^{2+}$ is displaced.[39] This change is within the estimated uncertainty of the fits, thus leaving open the question of whether Ca contributes to this peak.

In order to determine whether $Ca^{2+}$ contributes to the 3.3-Å feature, we have measured EXAFS data for $Sr^{2+}$-, $Dy^{3+}$-, and $La^{3+}$-substituted PSII reaction center complexes. In contrast to the report by Yachandra et al., we find that there are only very minor changes in the EXAFS for both the $Sr^{2+}$- and $Dy^{3+}$-substituted samples. We identify some of the possible difficulties associated with fitting these data and address the more general question of the reliability of EXAFS for structural analyses at long distances.

## Experimental Section

**Sample Preparation.** Reaction center complexes were isolated from spinach as previously reported resulting in highly active (1000−1400 $\mu$g of $O_2$/mg of chl/h) preparations lacking the light harvesting complex and the 17- and 23-kDa extrinsic polypeptides.[49,50] Samples were frozen at −80 °C prior to treatment. To prepare $Sr^{2+}$-substituted samples, the reaction center complex (approximately 2 mg chlorophyll) was first concentrated by centrifugation (40000*g*, 10 min), resuspended in 50 mM MES, 10 mM $SrCl_2$ (pH 6) to a final concentration of 0.66 mg chl/mL, and incubated with stirring for 60 min at 4 °C. The reaction center was reconcentrated by another centrifugation, and the pellet was packed into a lucite EXAFS cell, covered with polypropylene film, and frozen in liquid nitrogen. A portion of the pellet was saved for EPR characterization. The $Dy^{3+}$- and $La^{3+}$-substituted samples were prepared by resuspending the initial pellet to a concentration of 0.66 mg of chl/mL in 50 mM MES. An equal volume of 4 mM $LnCl_3$, 400 mM NaCl was added to this suspension and incubated for 60 min with stirring at 4 °C. Aliquots were saved for EPR characterization and the remaining sample was pelleted for the EXAFS sample cell. A calcium-depleted sample was prepared by subjecting the pellet to 2 cycles of washing in a $Ca^{2+}$-free buffer (50 mM MES). A standard Clark-type oxygen electrode was used to assay enzymatic activity. The remaining pellet was resuspended in 50 mM MES for activity assays. Assays were conducted in a 50 mM MES (pH 6) buffer containing either 10 mM $CaCl_2$ or 10 mM NaCl using 0.31 mM 2,6-dichlorobenzoquinone as an acceptor.

**EXAFS Measurements.** Mn K edge X-ray absorption spectra were measured at the Stanford Synchrotron Radiation Laboratory on beamline 7−3 using Si[220] crystals. X-ray absorption measurements were made at 10 K using an Oxford Instruments liquid He flow cryostat. Harmonic rejection was achieved by detuning the monochromator 50% at 7100 eV. The beamline was equipped with a Canberra 13-element solid state Ge detector for monitoring the Mn K$\alpha$ fluorescence. Spectra were calibrated by simultaneously measuring the absorption spectrum of $KMnO_4$; the distinctive $KMnO_4$ preedge feature was assigned a value of 6543.3 eV. Data collection parameters were described in the preceding paper.[36] Two sets of data for separately prepared $Dy^{3+}$- and $Sr^{2+}$-substituted samples have been collected and analyzed with identical results. A single data set for a $La^{3+}$-substituted sample has also been collected.

**Data Analysis.** EXAFS data reduction and data analysis procedures have been described elsewhere.[36,38] As narrow Fourier filtering can perturb the EXAFS spectra by introducing truncation effects,[51] only wide filters were used (over the three major FT peaks, 0.8−3.3 Å). All filtered fits discussed in this paper were verified with fits to the unfiltered data with equivalent results. The presence of Fe in PSII necessarily restricts the usable range of data to about $k = 1.5-11.5$ Å$^{-1}$. As described in detail elsewhere,[36] we find that the minimum requirements for fitting the control OEC are one shell of oxygens at ca. 1.85 Å, one shell of Mn scatterers at 2.72 Å, and one shell of metal scatterers at 3.3 Å. As we have noted previously,[36] the single Mn−O nearest neighbor shell cannot be a complete description of the Mn coordination environment in the OEC. However, additional shells of nearest neighbors (Cl or O) are not *required* to fit the data and have not been included for discussion in this paper. This leads to an unrealistically low apparent first-shell coordination number, most likely reflecting static disorder in the nearest neighbor distances. Details and discussion of these fits are given elsewhere.[36]

For each shell of scatterers, the only variable parameters were the distance, *R*, and the root-mean-square deviation in distance (the Debye−Waller factor), $\sigma$. All reasonable values of coordination numbers were tried, using integral values of 1−6 for the first shell of Mn−O/N scattering, using 1, 1.25, or 1.5 Mn−Mn interactions for the second shell, and using 0.25, 0.5, 0.75, or 1.0 Mn−X interactions for the third shell. The fits reported in Tables 2 and 3 are for the coordination numbers giving the best fit. For all data sets, including the controls, fits where X = Ca, Mn, C, Sr, or Dy were tried. Single-scattering and multiple-scattering theoretical parameters were generated with FEFF3.25 and FEFF5.04.[52,53] Based on fits to crystallographically characterized high-valent Mn dimers,[54] the optimum values for $\Delta E_0$ and the scale factor were found to be 10 eV and 0.9, respectively.

**EPR Spectroscopy.** X-band (9.2 GHz) Electron Paramagnetic Resonance (EPR) spectra were obtained using a Bruker ER 200E-SRC system equipped with a Bruker microwave bridge (model ER041MR) and a TM104 cavity. Helium temperatures were obtained with an Oxford continuous flow cryostat (FR0195 ESR900). Microwave frequency was monitored with a Hewlett Packard 5350B frequency counter. Data were collected using EPRWare (Scientific Software Services). Instrument settings are given in the figure legends.

(44) Riggs-Gelasco, P. J.; Stemmler, T. L.; Penner-Hahn, J. E. *Coord. Chem. Rev.* In press.
(45) Scott, R. A.; Eidsness, M. K. *Comments Inorg. Chem.* **1988**, *7*, 235−267.
(46) Fay, M. J.; Proctor, A.; Hoffmann, D. P.; Hercules, D. M. *Anal. Chem.* **1988**, *60*, 1225A-1243A.
(47) Yachandra, V. K.; DeRose, V. J.; Latimer, M. J.; Mukerji, I.; Sauer, K.; Klein, M. P. In *Research in Photosynthesis*; Murata, N., Ed.; Kluwer Academic Publishers: Boston, 1992; Vol. II, pp 281−287.
(48) Yachandra, V. K.; DeRose, V. J.; Latimer, M. J.; Mukerji, I.; Sauer, K.; Klein, M. P. *Jpn. J. Appl. Phys.* **1993**, *32*, 523−526.
(49) Ghanotakis, D. F.; Demetriou, D. M.; Yocum, C. F. *Biochim. Biophys. Acta* **1987**, *891*, 15−21.
(50) Berthold, D. A.; Babcock, G. T.; Yocum, C. F. *FEBS Lett.* **1981**, *134*, 231−234.
(51) Lytle, F. W.; Sayers, D. E.; Stern, E. A. *Phys. B* **1989**, *158*, 701−722.
(52) Rehr, J. J.; Albers, R. C. *Phys. Rev.* **1990**, *B41*, 8139.
(53) Rehr, J. J.; de Leon, J. M.; Zabinsky, S. I.; Albers, R. C. *J. Am. Chem. Soc.* **1991**, *113*, 5135−5140.
(54) Riggs-Gelasco, P. J. Ph.D. Thesis, University of Michigan, 1995.

**Table 1.** Representative Oxygen Evolution Rates for Diffrent Treatments[a]

| sample | % activity in NaCl | % activity in $CaCl_2$ |
|---|---|---|
| control $S_1$ | 69 | 100 |
| $Sr^{2+}$ substituted | 38 | 73 |
| $Dy^{3+}$ substituted | 16 | 31 |
| $La^{3+}$ substituted | 18 | 20 |
| washed[b] | 37 | 79 |

[a] Rates relative to that for the control measured in MES/$CaCl_2$ (1110 $\mu$mol of $O_2$/mg of chl/mL). [b] Sample rinsed and pelleted several times in a calcium free buffer.

## Results

**Sample Characterization.** All X-ray absorption spectra were measured using an energy-resolving X-ray fluorescence detector. X-ray fluorescence can thus be used to determine the metal composition in the samples used for EXAFS measurements. None of the metal-substituted samples showed any detectable Ca K$\alpha$ X-ray fluorescence. Based on parallel measurements on a 10 mM reference and on control OEC samples, the Ca detection limit under these conditions was approximately 0.1 mM. The Mn concentration in all samples was approximately 2 mM based on analogous Mn K$\alpha$ measurements. For a stoichiometry of 4 Mn/complex, this means that a minimum of 80% of the $Ca^{2+}$ was displaced from these samples. This is, however, not a particularly useful measure of Ca replacement. The relatively poor detection limits do not allow us to distinguish between 80% and 100% Ca displacement and, in any event, previous spectroscopic studies with which we wish to make comparisons[17,28,39,43,47,48] do not report any metal quantitation. Most important, however, is the fact that elemental analysis alone cannot demonstrate that $Sr^{2+}$, $Dy^{3+}$, or $La^{3+}$ have bound, but only that $Ca^{2+}$ has been removed. For this reason, we have used activity and EPR properties as a more sensitive measure of $Ca^{2+}$ replacement.

$Sr^{2+}$ substitution results in decreased activity ($\approx$40% of control activity can be reconstituted by $Sr^{2+}$ incubation) that can be reversed by incubation in $CaCl_2$.[13,28,55] Lanthanide substitution results in irreversible inactivation.[56] Representative oxygen evolution rates after $Sr^{2+}$ and $Ln^{3+}$ substitution are given in Table 1. These values are consistent with those reported in the literature for $Ca^{2+}$-substituted samples. As expected, $Sr^{2+}$ substitution is reversible whereas the activities of the $Dy^{3+}$ and $La^{3+}$ samples are not affected by incubation with $Ca^{2+}$.

To verify that the loss in activity was a result of $Ca^{2+}$ replacement rather than damage to the Mn cluster, XANES of the substituted samples were compared to those of control samples. Figure 1 shows that the oxidation state of Mn is unaffected by $Ca^{2+}$ substitution with $Sr^{+2}$, $Dy^{3+}$, or $La^{3+}$. In addition, the Mn K$\alpha$ fluorescence intensity for the control and substituted samples are similar, indicating that very little Mn is released during the incubation process. In contrast to the substituted samples, calcium depletion results in an edge shift to lower energy (Figure 1D). Edge fits[57] to this spectrum are consistent with the presence of ca. 15 $\pm$ 10% Mn(II) (data not shown).

$Sr^{2+}$ substitution is known to favor formation of the $g \approx 4.1$ EPR signal over the $g \approx 2$ multiline signal in the $S_2$ state.[17,28] Figure 2A shows that replacement of $Ca^{2+}$ with $Sr^{2+}$ results in a large increase in the amplitude of the $g \approx 4.1$ signal. The

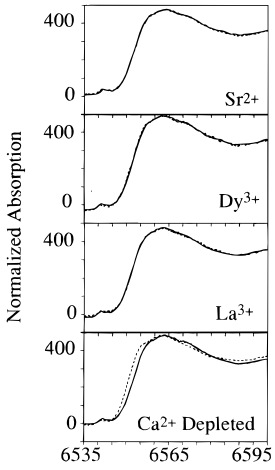


**Figure 1.** Normalized X-ray absorption near edge spectra for control samples (solid lines) vs $Ca^{2+}$-substituted samples (dashed lines): (A) $Sr^{2+}$-substituted sample, (B) $Dy^{3+}$-substituted sample, (C) $La^{3+}$-substituted sample, and (D) $Ca^{2+}$ depleted but not reconstituted with divalent cations.

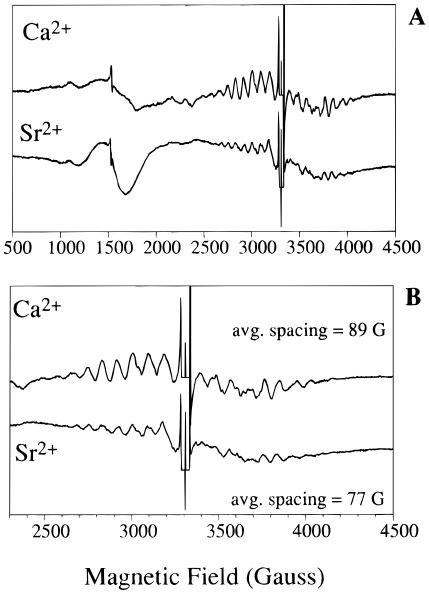


**Figure 2.** Part A: Light−dark difference EPR spectrum for untreated control sample vs a $Sr^{2+}$-substituted sample. Illumination for the control was done in a $CO_2$/acetone bath (200 K) in a clear glass dewar with a 400-W bulb for 10 min. The sample was then quenched in liquid nitrogen before being transferred to the liquid helium cryostat. Illumination of the $Sr^{2+}$-substituted sample was carried out in a $CO_2$/acetonitrile bath (230 K). Collection parameters were the following: 2500 G center field, 5000 G sweep width, 20 G peak-to-peak modulation amplitude, 20 ms time constant, 20.1 mW power, $2 \times 10^5$ gain, and 9.30 GHz frequency. Spectra were collected at 10 K and are the average of eight 200-s scans. Part B: Closeup of the multiline region centered at $g = 2$.

remaining multiline signal for the $Sr^{2+}$-substituted sample differs from that of the $Ca^{2+}$-containing control (Figure 2B). The average hyperfine coupling is decreased from $\approx$89 (control) to 77 G ($Sr^{2+}$ substituted) and the intensity patterns are altered. This is comparable to the effects reported previously for $Sr^{2+}$-substituted samples. There are minor differences in the low-field portion of our $g \approx 2$ signal; however, the high-field portion is identical to that reported previously.[17]

Lanthanide substitution completely displaces the $Ca^{2+}$ associated with PSII.[23,56] An indirect measure of lanthanide binding is the broadening of the hyperfine features of the EPR signal of the stable tyrosine radical, $Y_D^{\bullet}$.[23] Substitution of a

(55) Sivaraja, M.; Tso, J.; Dismukes, G. C. *Biochemistry* **1989**, *28*, 9459−9464.
(56) Bakou, A.; Ghanotakis, Demetrios F. *Biochim. Biophys. Acta* **1993**, *1141*, 303−308.
(57) Riggs, P. J.; Mei, R.; Yocum, C. F.; Penner-Hahn, J. E. *J. Am. Chem. Soc.* **1992**, *114*, 10650−51.

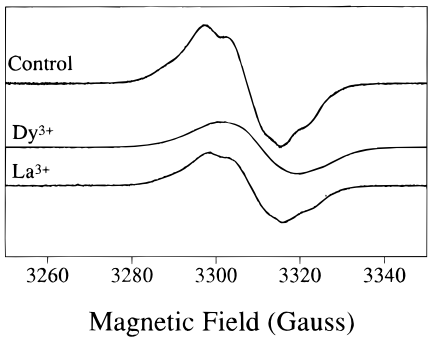


**Figure 3.** EPR spectra of the dark stable tyrosine radical in a control $S_1$ sample, a $Dy^{3+}$-substituted sample, and a $La^{3+}$-substituted sample. Collection parameters were as follows: 3300 G center field, 200 G sweep width, 4 G peak-to-peak modulation amplitude, 20.1 mW power, 8000 gain, 10 ms time constant, 9.29 GHz frequency. Spectra were collected at 10 K and are a single 100-s sweep.

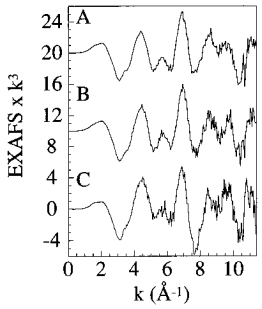


**Figure 4.** Comparison of $k^3$ weighted EXAFS spectra for untreated control $S_1$ sample (A), $Sr^{2+}$-substituted sample (B), and $Dy^{3+}$-substituted sample (C). Data are offset vertically for clarity. Data in C are corrected for detector deadtime response.

paramagnetic lanthanide ($Dy^{3+}$) produces a featureless signal while a diamagnetic lanthanide ($La^{3+}$) does not give any broadening. Figure 3 shows the effect of $Dy^{3+}$ and $La^{3+}$ substitution on the EPR spectrum of $Y_D^{\bullet}$.

**EXAFS Measurements.** Figure 4 shows the unfiltered EXAFS data for a control $S_1$ sample, a $Sr^{2+}$-substituted sample, and a $Dy^{3+}$-substituted sample. The resulting Fourier transforms are displayed in Figure 5. There is no major change in the Mn cluster structure for the $Sr^{2+}$- and $Dy^{3+}$-substituted samples. In particular, we do not observe any increase in the size of the peak at $R + \alpha \approx 3.0$ Å. The single $La^{3+}$-substituted sample (data not shown) was not useful for this comparison because of the noise level.[58]

Fits to both the filtered (R=0.8−3.3 Å) and the unfiltered data utilized either three (Mn, O, M) or four (Mn, O, M, C) shells of scatterers, where M = Mn, Sr, or Dy. Additional fits using Ca rather than Mn at 3.3 Å gave results that were identical to those for Mn···Mn, aside from a slight decrease in the apparent Mn···M distance. This is not surprising, given the close similarity of Mn···Mn and Mn···Ca scattering (see below). Average fitting results for two independent data sets of the $Sr^{2+}$-substituted samples and their corresponding controls are given in Table 2. Table 3 gives results for two independent $Dy^{3+}$-substituted data sets and corresponding controls. Since the 3.3-Å feature does not change when $Ca^{2+}$ is replaced (see below), Mn···Mn is the most likely contributor at this distance, and the Mn···Mn rather than the Mn···Ca results are included in Tables 2 and 3.

(58) The proximity of the La L-edge fluorescence lines to the Mn Kα fluorescence line made it necessary to narrow the Mn fluorescence window, thus decreasing the count rate significantly relative to the control and other substituted samples. The 3.3-Å peak is not significantly above the noise level in this spectrum.

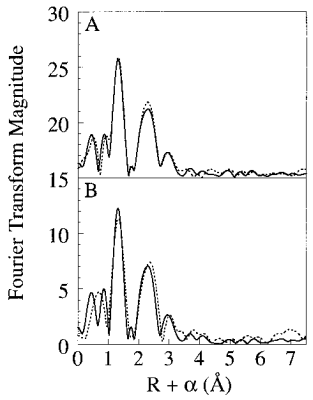


**Figure 5.** Fourier transforms of $S_1$ EXAFS spectra: (A) control (solid line) vs $Sr^{2+}$-substituted sample (dashed line); (B) control (solid line) vs $Dy^{3+}$-substituted sample (dashed line). Both spectra in B were corrected for deadtime response. Fourier transforms were calculated over a $k$ range of 1.5−11.4 (A) or 11.5 $Å^{-1}$ (B). Each control spectrum was measured at the same time as its corresponding $Ca^{2+}$-substituted spectrum. Duplicate measurements for each pair of spectra (not shown) give identical results.

For all of the data sets, the dominant EXAFS contributions are from nearest neighbor Mn−O and next-nearest neighbor Mn···Mn scattering. There are no EXAFS detectable perturbations in the first shell (Mn−O interactions) following the substitutions. However, there are small changes in the 2.7-Å feature. The average Mn···Mn distance decreases slightly in the $Sr^{2+}$-substituted samples (from 2.726 to 2.712 Å) and increases somewhat in the $Dy^{3+}$-substituted samples (from 2.723 to 2.734 Å). The trend in the ≈2.7-Å Mn−Mn distance is reproducible for independently prepared and measured samples, as summarized in Table 4. The trend is not dependent on the identity of the scatterer that is used to fit the third ($R \approx 3.3$ Å) shell or on the use of filtered vs unfiltered data.

Results for the fitting analysis for the third (Mn···M) and fourth (Mn···C) shells for the $Sr^{2+}$- and $Dy^{3+}$-substituted samples and their corresponding controls are also summarized in Tables 2 and 3. Representative three-shell fits are shown in Figures 6 (fits A and C for a control sample) and 7 (fits F and H for a $Sr^{2+}$-substituted sample). The third peak in the Fourier transform can be fit using only Mn···C or Mn···M (M = Ca, Mn, Sr, or Dy) interactions at ca. 3.3 Å, although the Mn···M fits are better. There is an alternate minimum at approximately 3.7 Å, but these fits are consistently ca. 10% worse in quality than those that place the scatterer at 3.3 Å.

Inclusion of Mn···C scattering at 3.0 Å in addition to Mn···M scattering at 3.3 Å results in slightly better fits (slightly lower $F$ values) in all cases. However, the improvement in fit quality is not significant enough to reliably define a Mn···C shell. We have previously[36] introduced a modified fit index, $F' = F^2/\nu$, where $\nu$ is the number of unused degrees of freedom (i.e., the number of independent data points minus the number of variables). $F'$ is an attempt to account for the improvement in fit quality that occurs simply as a consequence of using a larger number of variable parameters. Inclusion of the Mn···C shell gives a worse fit, as judged by $F'$ in all cases except fits C2/D2 and F2/G2. In the latter cases, $F'$ is unchanged by inclusion of the Mn···C shell. There is thus no evidence that the Mn···C shell is required. Fits using Mn···C are nevertheless included in Tables 2 and 3 in order to illustrate that our conclusions (below) do not depend on inclusion/omission of the Mn···C shell.

Attempts to fit the 3.3-Å peak with Mn−Mn + Mn−Ca scattering do not give any significant improvement in fit quality, as judged by either $F$ or $F'$ (data not shown). In these fits,

**Table 2.** Average Fitting Results for $Sr^{2+}$-Substituted Samples and Corresponding Controls[a]

| | | | Mn−O/N | | | Mn···Mn | | | Mn···M[b] | | | Mn···C | | | fit quality[c] | |
|---|---|---|---|---|---|---|---|---|---|---|---|---|---|---|---|---|
| sample | fit label | and type | $R$ (Å)[d] | CN[e] | $\sigma^2$ [f] | $R$ (Å) | CN | $\sigma^2$ | $R$ (Å) | CN | $\sigma^2$ | $R$ (Å) | CN | $\sigma^2$ | $F_1$ | $F_2$ |
| control | A | O, Mn, Mn | 1.855(1) | 3 | 7(1) | 2.726(2) | 1 | 1(1) | 3.25(1) | 1 | 6(4) | | | | 0.552 | 0.418 |
| | B | O, Mn, Mn, C | 1.854(9) | 3 | 7(1) | 2.728(2) | 1.5 | 3(1) | 3.25(1) | 1 | 7(1) | 2.98(3) | 3.5 | 9(1) | 0.512 | 0.414 |
| | C | O, Mn, Sr | 1.856(10) | 3 | 7(2) | 2.725(1) | 1 | 2(1) | 3.11(0) | 1 | 9(1) | | | | 0.539 | 0.465 |
| | D | O, Mn, Sr, C | 1.856(11) | 3 | 7(1) | 2.729(3) | 1.25 | 2(1) | 3.12(1) | 0.5 | 5(3) | 3.04(4) | 2.5 | 12(9) | 0.521 | 0.423 |
| | E | O, Mn, C | 1.856(9) | 3 | 7(1) | 2.726(1) | 1 | 2(2) | | | | 3.25(1) | 2 | 2(2) | 0.599 | 0.482 |
| $Sr^{2+}$ | F | O, Mn, Mn | 1.852(8) | 3 | 7(1) | 2.712(0) | 1 | 2(1) | 3.26(3) | 1 | 9(0) | | | | 0.388 | 0.294 |
| | G | O, Mn, Mn, C | 1.851(5) | 3 | 7(1) | 2.715(2) | 1.5 | 3(1) | 3.25(1) | 0.75 | 6(3) | 2.98(1) | 4 | 21(3) | 0.367 | 0.251 |
| | H | O, Mn, Sr | 1.852(6) | 3 | 7(1) | 2.711(1) | 1 | 2(1) | 3.09(1) | 1 | 10(0) | | | | 0.392 | 0.353 |
| | I | O, Mn, Sr, C | 1.851(6) | 3 | 7(1) | 2.717(1) | 1.5 | 4(1) | 3.11(1) | 1 | 10(1) | 3.03(2) | 3 | 13(1) | 0.366 | 0.306 |
| | J | O, Mn, C | 1.852(5) | 3 | 7(1) | 2.714(1) | 1 | 2(1) | | | | 3.24(0) | 2 | 3(1) | 0.464 | 0.413 |

[a] Best fit results for each model type. The refined parameters ($R$ and $\sigma^2$) are the average for two independent data sets, with the rms deviation in the last digit given in parentheses. Data are not corrected for dead time response. [b] M = either Mn or Sr. [c] rms deviations for two independent data sets; $F = [\sum k^6(\chi_{obs} - \chi_{calc})^2/N]^{1/2}$ where $N$ = number of data points. Subscript on $F$ refers to data set 1 or 2. [d] $R$ is apparent absorber−scatter distance. [e] CN is integer (or quarter integer for M···M) coordination number giving the best fit. [f] $\sigma^2$ is Debye−Waller factor × $10^3$ in units of Å$^2$.

**Table 3.** Average Fitting Results for $Dy^{3+}$-Substituted Samples and Corresponding Controls[a]

| | | | Mn−O/N | | | Mn···Mn | | | Mn···M[b] | | | Mn···C | | | fit quality[c] | |
|---|---|---|---|---|---|---|---|---|---|---|---|---|---|---|---|---|
| sample | fit label | and type | $R$ (Å)[d] | CN[e] | $\sigma^2$ [f] | $R$ (Å) | CN | $\sigma^2$ | $R$ (Å) | CN | $\sigma^2$ | $R$ (Å) | CN | $\sigma^2$ | $F_1$ | $F_2$ |
| control | K | O, Mn, Mn | 1.856(1) | 3 | 7(1) | 2.723(2) | 1 | 2(1) | 3.27(1) | 1 | 9(3) | | | | 0.701 | 0.724 |
| | L | O, Mn, Mn, C | 1.855(1) | 3 | 7(1) | 2.722(3) | 1.5 | 2(1) | 3.27(2) | 1 | 9(2) | 2.96(2) | 3.5 | 21(15) | 0.642 | 0.691 |
| | M | O, Mn, Dy | 1.855(1) | 3 | 7(1) | 2.722(1) | 1 | 2(1) | 3.41(2) | 1 | 9(3) | | | | 0.639 | 0.785 |
| | N | O, Mn, Dy, C | 1.855(1) | 3 | 7(1) | 2.719(1) | 1.25 | 2(1) | 3.40(1) | 0.75 | 5(1) | 2.91(1) | 3 | 3(3) | 0.607 | 0.755 |
| | O | O, Mn, C | 1.853(1) | 2.5 | 5(3) | 2.723(1) | 1 | 2(1) | | | | 3.27(1) | 2 | 4(4) | 0.705 | 0.769 |
| $Dy^{3+}$ | P | O, Mn, Mn | 1.864(1) | 3 | 5(1) | 2.734(1) | 1 | 2(1) | 3.26(2) | 0.75 | 9(5) | | | | 0.704 | 0.590 |
| | Q | O, Mn, Mn, C | 1.863(1) | 3 | 3(1) | 2.738(2) | 1 | 3(1) | 3.25(1) | 1 | 9(0) | 3.01(2) | 3 | 8(1) | 0.657 | 0.546 |
| | R | O, Mn, Dy | 1.863(1) | 3 | 5(1) | 2.735(1) | 1 | 2(1) | 3.37(1) | 1 | 9(0) | | | | 0.679 | 0.563 |
| | S | O, Mn, Dy, C | 1.863(1) | 3 | 5(1) | 2.736(1) | 1.5 | 4(1) | 3.37(1) | 1 | 8(0) | 2.97(2) | 3 | 9 | 0.667 | 0.552 |
| | T | O, Mn, C | 1.863(1) | 3 | 5(2) | 2.737(1) | 1 | 3(1) | | | | 2.96(1) | 2 | 5 | 0.720 | 0.615 |

[a] Best fit results for each model type. The refined parameters ($R$ and $\sigma^2$) are the average for two independent data sets, with the rms deviation in the last digit given in parentheses. Data are corrected for dead time response. [b] M = either Mn or Dy. [c] rms deviations for two independent data sets; $F = [\sum k^6(\chi_{obs} - \chi_{calc})^2/N]^{1/2}$ where $N$ = number of data points. Subscript on $F$ refers to data set 1 or 2. [d] $R$ is apparent absorber−scatter distance. [e] CN is integer (or quarter integer for M···M) coordination number giving the best fit. [f] $\sigma^2$ is Debye−Waller factor × $10^3$ in units of Å$^2$.

**Table 4.** Change in 2.7 Å Interaction for Independent Data Sets

| sample | $\Delta R_{Mn\cdots Mn}$[a] |
|---|---|
| Sr-1 | −0.015 |
| Sr-2 | −0.012 |
| Dy-1 | +0.011 |
| Dy-2 | +0.013 |

[a] Change in Mn···Mn distance for the control and $Ca^{2+}$-substituted samples measured under identical conditions.

either the amplitude of one shell refines to zero (e.g., a very large Debye−Waller factor) or the shells refine to distances that are too close (e.g. 0.10 Å) to be distinguished within the limited resolution of these data.

If a Mn···Mn interaction is used to describe the 3.3-Å feature in a control sample or in the substituted samples, an apparent Mn···Mn distance of ≈3.25 Å is obtained. If Sr scattering is used to fit this feature in either a control or a $Sr^{2+}$-substituted sample, the apparent distance refines to a much shorter value (≈3.10 Å). For the $Dy^{3+}$-substituted sample, the third shell can be modeled with Mn···Dy interactions at 3.34−3.36 Å. If the control sample is modeled with a Mn···Dy interaction, the distance also refines to 3.34−3.36 Å.

In no cases does the fit quality depend significantly on the identify of the scatterer included at approximately 3.3 Å. For one control data set and both data sets for the $Sr^{2+}$-substituted samples, the three shell fits with Sr are slightly worse fit than the corresponding three-shell fits utilizing Mn (see Table 2). However, one of the control data sets shows a slight *improvement* when its 3.3-Å feature is modeled with Sr. Three shell fits to both data sets for the $Dy^{3+}$-substituted samples are slightly better if Dy is used rather than Mn (see Table 3). For the corresponding controls, one data set is fit slightly better with Dy while one is fit slightly better with Mn. Adding a fourth shell of carbon does not change any of the fits significantly and does not give a significant improvement in any of the fits. However, the use of a carbon shell does change the optimal metal scatterer from Dy to Mn in the $Dy^{3+}$-substituted data sets.

## Discussion

**Effectiveness of Metal Replacement.** There is substantial variability in published protocols for calcium depletion. Most of the reported protocols utilize some combination of chelator, pH treatment, light, and high salt concentrations. Consequently, there have been apparently contradictory reports of the properties of the multiline signal and of the ability to form the $S_3$ 164-G signal.[10] For example, Boussac et al. demonstrated that samples depleted of calcium with 1.2 M NaCl treatment in the light, followed by treatment with 50 $\mu$M EGTA, do not form the dark stable, altered multiline signal.[32] If, however, these samples were exposed to high (10 mM) concentrations of EGTA or citrate (pH 6.5, 40 mM), then modifications to the multiline signal were observed. Dark treatment with citrate at pH 3 did not result in the altered multiline signal until the sample was exposed to continuous illumination at high temperatures (> −5 °C).[31] The observation of a dark stable, modified $S_2$ state requires the use of both light and chelators at high concentrations but does not depend on the presence of the extrinsic polypeptides.[10,32]

In this study, we sought to isolate the structural perturbations due to cation substitution from those which might arise from

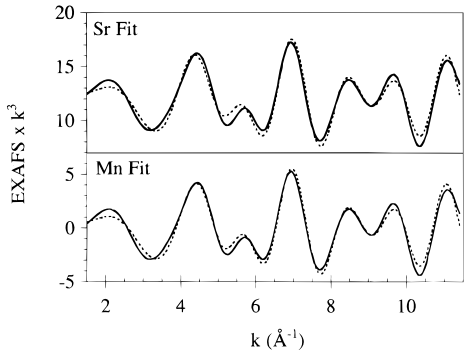


**Figure 6.** Representative fits for a control sample not corrected for deadtime response. The fits are to data (solid lines) filtered over a wide range in the Fourier transforms (0.8−3.3 Å). The top frame is a three-shell fit (dashed line) incorporating one shell of Mn−O, one shell of Mn···Mn at 2.7 Å, and a Mn···Sr interaction at 3.15 Å. The bottom frame is the three-shell fit (dashed line) to the same data; however, in this case the third shell peak is modeled with a Mn···Mn interaction. Fitting details are given in Table 2.

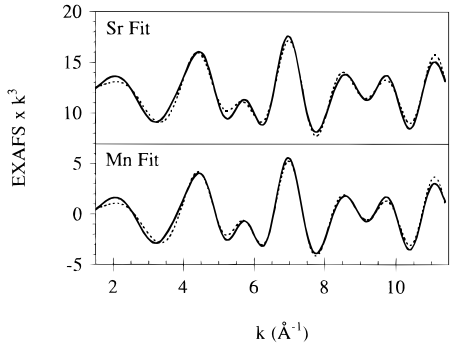


**Figure 7.** Representative fits for a $Sr^{2+}$-substituted sample not corrected for detector deadtime response. Both fits (dashed lines) are three-shell fits to the same data (solid lines) filtered over a wide range in the Fourier transforms (0.8−3.3 Å). The top frame utilized a Mn···Sr interaction to model the third shell. The bottom frame utilized a Mn···Mn interaction. Fitting details are given in Table 3.

chelator binding to the Mn cluster,[32] and, therefore, employed a simple wash/incubation protocol for metal substitution. The starting preparation was already depleted of the extrinsic polypeptides, so high salt concentrations were not necessary to lower the affinity of calcium for its binding site(s). Since we did not make use of high salt concentrations or chelators, it was important to demonstrate successful $Ca^{2+}$ substitution in our preparations. The efficacy of our approach is demonstrated for $Sr^{2+}$ substitution by the observation of reversible inhibition of activity[13,28,55] and by the stabilization of the $g \approx 4.1$ $S_2$ EPR signal relative to the multiline signal.[28] The multiline signal also showed the expected changes in hyperfine spacing and redistributions of line intensity (see Figure 2B).[28,59] Lanthanide substitution (with $Dy^{3+}$ or $La^{3+}$) was achieved using a modification of the procedure of Bakou et al.[23] The changes that are expected to be associated with $Ln^{3+}$ substitution were observed. The activity was irreversibly inhibited and binding of the paramagnetic $Dy^{3+}$ induced a broadening of the hyperfine features of the $Y_D^{\bullet}$ EPR signal.

The XANES spectra of the substituted samples (Figure 1) demonstrate that no oxidation state changes were associated with the metal replacements. In particular, the identity of the XANES spectra for the $Ca^{2+}$-substituted samples demonstrates that there was no adventitiously bound $Mn^{2+}$, that might have been released during the incubation process.

A third line of evidence demonstrating the efficacy of our $Ca^{2+}$ substitution is the reproducible change that is observed in the 2.7-Å Mn···Mn distance following $Ca^{2+}$ replacement (see Tables 2 and 3). This change has not previously been reported. The change in Mn···Mn distance is small (see below) but highly reproducible. This demonstrates that a systematic, reproducible structural change takes place as a result of $Ca^{2+}$ replacement. Taken together, these results demonstrate that our wash/incubation protocol gives samples that are equivalent to other $Ca^{2+}$-substituted samples.

In contrast to the $Sr^{2+}$-, $Dy^{3+}$-, and $La^{3+}$-substituted samples, where the XANES spectrum was unaffected by $Ca^{2+}$ substitution, the calcium-depleted sample, where $Ca^{2+}$ is replaced by $Na^{+}$, shows a significant edge shift to lower energy. Edge fits to this spectrum are consistent with the presence of up to 15% Mn(II). Comparable edge shifts have been reported previously following $Ca^{2+}$ depletion.[39,43,60] These have been attributed to conformational rather than oxidation state changes,[39] based on the lack of a detectable 6-line EPR signal from Mn(II). However, the Mn that is released from inactive centers is known to bind to the OEC and to be largely undetectable by EPR in the absence of added $Ca^{2+}$.[61] It is thus possible that the edge shift that is observed following $Ca^{2+}$ depletion may be the consequence of $Mn^{2+}$ occupying the $Ca^{2+}$ binding site or other adventitious sites on the OEC.[13,25,26] In the presence of $Ca^{2+}$ (or competing cations), this inactive Mn(II) is displaced from the OEC and does not contribute to the XANES spectrum.[36,62] This interpretation is consistent with the observation that only partial activity is restored when $Ca^{2+}$ is added to the $Ca^{2+}$-depleted sample. Based on activity, we estimate that ≈20% of the centers have lost functional Mn clusters during $Ca^{2+}$ removal (see Table 1). Because of this apparent heterogeneity (i.e., active centers + $Mn^{2+}$), we have not analyzed the EXAFS data for the $Ca^{2+}$-depleted samples.

**The 3.3-Å Interaction.** As discussed above, the outer-shell scattering has been assigned to scatterers at ca. 3.3 Å[33,35,36,38,41−43] or ca. 3.7 Å.[34,39] This difference has been attributed to differences in methods of data analysis.[35,39] In particular, Nugent and co-workers have suggested[39] that the use of curved-wave ab initio parameters gives rise to their 3.7-Å distance. However, we have used similar curved-wave parameters and continue to find a distance of ca. 3.3 Å. It is possible that the difference is due to differences in the programs used to calculate the EXAFS parameters. Thus, recent work[63] has suggested that EXCURVE, the program used by Nugent and co-workers, may give large errors in amplitude and phase, in comparison with FEFF. Alternatively, it may be that the 3.3- vs 3.7-Å distances represent alternate minima in the fit space. We find that it is possible to fit our data using a shell at ca. 3.7 Å, but that these fits are consistently worse than fits at 3.3 Å.

It is possible to model the 3.3-Å feature as arising in part from a combination of Mn···Mn and Mn···Ca interactions.[41,43] However, we do not find any significant changes either in the FT peak intensity or in the curve-fitting results when $Ca^{2+}$ is replaced by other metals. Since the variations in EPR spectra, in activity, and in the 2.7-Å Mn···Mn distances all suggest that

(59) In principle, $Sr^{2+}$ that is bound to the OEC in solution might be displaced on pelleting. However, EPR and EXAFS measurements were both performed on pelleted samples. Moreover, activity assays on resuspended pellets and were identical to assays done without pelleting. These observations demonstrate that the pelleting process does displace $Sr^{2+}$ from the $Ca^{2+}$ binding site.

(60) Ono, T.-A.; Kusunoki, M.; Matshshita, T.; Oyanagi, H.; Inoue, Y. *Biochemistry* **1991**, *30*, 6836−6841.
(61) Yocum, C. F.; Yerkes, C. T.; Blankenship, R. E.; Sharp, R. R.; Babcock, G. T. *Proc. Natl. Acad. Sci. U.S.A* **1981**, *78*, 7507−11.
(62) Mei, R.; Yocum, C. F. *Biochemistry* **1991**, *30*, 7836−7842.
(63) Vaarkamp, M.; Dring, I.; Oldman, R. J.; Stern, E. A.; Koningsberger, D. C. *Phys. Rev. B* **1994**, *50*, 7872−83.

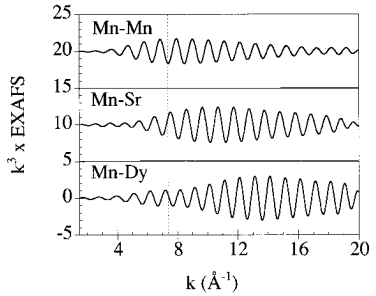


**Figure 8.** Comparison of the shape of amplitude envelopes and phases of theoretical simulations of Mn···Mn, Mn···Sr, Mn···Ca, and Mn···Dy EXAFS. Simulations calculated using FEFF5.04 for a single interaction at 3.3 Å with a $\sigma^2$ value of 0.0025 Å$^2$. Vertical line is drawn to facilitate phase comparisons between the traces.

$Ca^{2+}$ replacement was successful, the absence of detectable changes in the EXAFS interactions at 3.3 Å leads to three possible conclusions: (1) there is a Mn···Ca at 3.3-Å interaction that is not disrupted by $Sr^{2+}$ or $Dy^{3+}$ replacement, (2) there are Mn···Sr or Mn···Dy interactions at ca. 3.3 Å but they are not sufficiently different from the native Mn···Ca interaction to be EXAFS detectable, or (3) the native structure does not contain an EXAFS detectable 3.3-Å Mn···Ca interaction.

The first of these options seems unlikely. It is inconsistent with the lack of detectable Ca in our metal-substituted samples. In addition, if there is only a single $Ca^{2+}$ site that is required for $O_2$ evolution, it is unlikely that this site is *more* distant from the Mn than a putative, non-exchangeable site 3.3 Å from the Mn. Most importantly, it is clear that we have substituted the *same* $Ca^{2+}$ that has been implicated in the changes in activity and EPR spectra. If there is a $Ca^{2+}$ at 3.3 Å from the Mn that is not replaced under our conditions, this is not the $Ca^{2+}$ that is responsible for the standard perturbations in activity and EPR spectra.

To address the question of the sensitivity of EXAFS, we simulated Mn···Ca, Mn···Mn, Mn···Sr, and Mn···Dy interactions at 3.3 Å with the program FEFF5.0.[52,53] As expected, Mn and Ca give nearly identical EXAFS. This is why our fits were unable to distinguish between these two scatterers. In contrast, there are significant differences in the amplitude envelopes for Mn···Mn/Ca, Mn···Sr, and Mn···Dy (see Figure 8), with the maximum in the amplitude envelope shifting to increasingly higher *k* as the atomic weight of the scatterer increases. Note, however, that if the *k* range is limited to that used in OEC EXAFS studies (1.5−11.5 Å$^{-1}$), the differences in the amplitude envelope are not nearly as apparent. This is reflected in the resulting FT amplitudes for the two different *k* ranges (Figure 9). If the FT is calculated over $k = 1.5-20$ Å$^{-1}$ there are significant differences between the scatterers, but when the range is restricted to that used for the OEC (1.5−11.5 Å$^{-1}$), the four different FTs look much more similar. Interpretation of the protein data may be further complicated by interference between Mn···M and Mn···C scattering and by the noise level of the data. Thus, using a limited *k* range, a 3.3-Å interaction that is due primarily to Mn···Ca scattering is not expected to exhibit a significant change in peak *amplitude* if $Ca^{2+}$ is replaced by $Sr^{2+}$ or $Dy^{3+}$.

It is important to remember, however, that EXAFS consists of both amplitude and phase information. Although there are only small changes in the EXAFS amplitude, as shown by the magnitude of the FTs in Figure 9B, there are significant changes in the EXAFS phase on going from Mn···Mn/Ca to Mn···Sr to Mn···Dy (see Figure 8). As a consequence, replacement of $Ca^{2+}$ with $Sr^{2+}$ or $Dy^{3+}$ could conceivably give a large increase in FT amplitude if the 3.3-Å feature contains contributions from

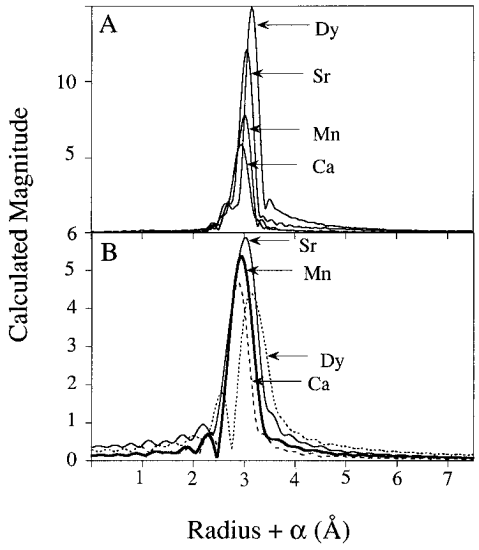


**Figure 9.** Fourier transforms of ab initio EXAFS parameters shown in Figure 8. Part A is a transform calculated over a *k* range of 1.5−20 Å$^{-1}$. Part B is a transform calculated from 1.5 to 11.5 Å$^{-1}$.

both Mn···M and Mn···C components. This would happen if the replacement of M with an alternate metal caused the Mn···M + Mn···C interference to change from destructive to constructive.

The theoretical simulations described above suggest that it is likely to be difficult to distinguish Sr and Dy backscatterers from a Ca backscatterer under the limitations of protein EXAFS. This is perhaps not surprising, given that even M···M and M···C scattering are sometimes not readily distinguishable by EXAFS.[45] The fitting results for the third shell (summarized in Tables 2 and 3) reflect this ambiguity. There are only small changes in fit quality when the 3.3-Å feature in the control samples is fit with Mn, Sr, or Dy. Most telling is the observation that some of the control samples give better fits with Sr or Dy than with Mn or Ca at 3.3 Å, despite the impossibility of Sr or Dy scattering in the control samples. This demonstrates that changes in fit quality alone cannot be used as a reliable measure of the identity (Ca, Mn, Sr, or Dy) of the scatterer at 3.3 Å, at least not with data over a limited *k* range.

Fortunately, fit quality is not the only measure that can be used to distinguish between possible backscatterers. The apparent Mn···M distances depend strongly on the identity of the scatterer used to model M. This is a consequence of the phase differences (see above) between Mn···Ca/Mn, Mn···Dy, and Mn···Sr EXAFS. If the data for either a control sample *or* a $Sr^{2+}$-substituted sample are fit with a Mn···Sr component at ≈3.3 Å, the refined Mn···Sr distance is ca. 3.1 Å. This is significantly shorter than the apparent Mn···Mn distance (3.25 Å) that is found for these samples. Likewise, if any of the data sets are sample modeled with Mn···Dy scattering, the apparent Mn···Dy distance (3.36 Å) is significantly lengthened relative to the Mn···Mn distance.

Identical results are obtained for simulated data fit with the "wrong" scatterer. The simulated EXAFS spectra in Figure 8 were fit over the *k* range 1.5−11.5 Å$^{-1}$ with each of the possible scatterers (Mn, Sr, or Dy). If the Mn···Mn scatterer was modeled with Sr, the refined distance was 3.17 Å; if it was modeled with Mn···Dy, the refined distance was 3.35 Å. Attempts to fit Mn···Mn scattering with Sr gave an apparent Mn···Sr distance that was ≈0.13 Å too short while attempts to fit Mn···Sr scattering with Mn gave an apparent Mn···Sr distance that was ≈0.13 Å too long. Analogous results were obtained for Mn and Dy, although here the error in distance

**Table 5.** Variation in Apparent Mn···M Distances as a Function of M[a]

| | $\Delta R$ (Å) with data from | | | |
|---|---|---|---|---|
| fit with | Mn···Mn | Mn···Sr | Mn···Dy | $[Mn^{III}(salpn)(OCH_3)]_2$ |
| Mn···Mn | 0.0 | +0.13 | −0.05 | +0.02 |
| Mn···Sr | −0.13 | 0.0 | −0.30 | −0.11 |
| Mn···Dy | +0.05 | +0.43 | 0.0 | +0.05 |

[a] Tabulated values are the error in apparent bond length for theoretical (Mn···Mn, Mn···Sr, and Mn···Dy) and empirical Mn···Mn ($[Mn^{III}(salpn)(OCH_3)]_2$) interactions at ca. 3.3 Å. Fits were over a $k$ range of 1.5−11.5 $Å^{-1}$. Theoretical models were generated using FEFF5.04 using a $\sigma^2$ value of 0.0025 $Å^2$. Phase and amplitude functions for fits were derived from FEFF3.25 and were identical to those used in the protein fitting analysis.

was only 0.05 Å. Similar errors in the apparent Mn···M distance were found when the authentic 3.19-Å Mn···Mn interaction in $[Mn^{III}(salpn)(OCH_3)]_2$ was modeled with Sr or Dy scattering. These results are summarized in Table 5. The origin of these differences is the differences in EXAFS phase for the different absorber−scatterer pairs. The significance of these differences is that they provide an opportunity to distinguish between different scatterer types.

**Structural Implications.** If the 3.3-Å Mn···M component was due to an exchangeable $Ca^{2+}$ rather than being due to Mn, then the apparent Mn···Mn distance in the $Sr^{2+}$-substituted sample would be too long by about 0.13 Å as a consequence of modeling the Mn···Sr scattering with Mn···Mn parameters. Similarly, the apparent Mn···Mn distance in the $Dy^{3+}$-substituted sample would be an underestimate of the true Mn···Dy distance by about 0.05 Å. In contrast, we do not observe any change in the apparent ca. 3.3-Å Mn···Mn distance following either $Sr^{2+}$ or $Dy^{3+}$ substitution. We cannot, of course, rule out the possibility that there are compensatory changes in the Mn···M distance. Thus, if $Sr^{2+}$ substitution gave a Mn···Sr distance that was 0.13 Å shorter than a native Mn···Ca distance while $Dy^{3+}$ substitution gave a Mn···Dy distance that was 0.05 Å longer, there would be no change in the apparent Mn···Mn distance. However, these distances are inconsistent with those expected on the basis of ionic radii ($Sr^{2+}$ > $La^{3+}$ > $Ca^{2+}$ > $Dy^{3+}$). It thus appears to be very unlikely that there is an EXAFS detectable Mn···Ca distance in our samples. Since good fits to the 3.3-Å feature appear to require an Mn···M component, we believe that the native and both of the substituted samples have a Mn···Mn interaction at this distance. This is consistent with the disappearance of the 3.3-Å feature following reduction of Mn by hydroquinone in $Ca^{2+}$-saturated samples.[36]

**Variations in the 2.7-Å Mn−Mn Distance.** The observation of a small but reproducible change in the 2.7-Å interaction following $Ca^{2+}$ substitution demonstrates that $Ca^{2+}$ replacement causes a structural perturbation of the Mn cluster. In $Sr^{2+}$-substituted samples, the Mn···Mn distance decreases by approximately 0.014 Å relative to that in the control. In $Dy^{3+}$-substituted samples, the average Mn···Mn distance increases by approximately 0.012 Å, and in $La^{3+}$-substituted samples, there is an even larger increase in the average Mn···Mn distance, to ca. 2.78 Å (data not shown).[64] There also appear to be small changes in the average Mn−O distances when $Ca^{2+}$ is replaced by $Sr^{2+}$ or $Dy^{3+}$. These have the same sign, but approximately half of the magnitude ($\Delta R \approx 0.006$ Å), of the changes in Mn···Mn distance.

These subtle changes are somewhat smaller than the estimated accuracy of our measurements (±0.02 Å).[54] In the case of the Mn−O distances, the variations are reproducible, but too small to be interpreted with confidence. However, the variations in the Mn···Mn distance are approximately three times larger than the precision of our measurements. Samples were studied in pairs in order to control any small variations in the synchrotron beamline from run to run.[65,66] The reproducibility in Table 4 suggests that the change in Mn···Mn distance can be determined with a precision of about 0.003 Å. A more conservative estimate of the precision is obtained by ignoring possible variations from run to run, and simply averaging all of the control samples. In this case, the standard deviation in the Mn···Mn distance for six independent samples is about 0.005 Å,[36] which is still substantially smaller than the changes in Mn···Mn distance that are observed following $Ca^{2+}$ replacement. It thus appears likely that the variations in the apparent Mn···Mn distance are real.

Two factors could potentially cause the apparent Mn···Mn distance to change in the absence of a true change in the Mn···Mn separation. A 2−3-eV change in $E_0$ could account for the observed variation in Mn···Mn distance. However, this is inconsistent with the lack of any detectable change in the edge energy (see Figure 1). It is also possible that the addition of another scatterer (e.g., Mn···C) could result in a change in the apparent Mn···Mn distance. Although the data can be fit with an additional Mn···C shell at approximately 2.7 Å, this does not result in a significantly better fit or a significant change in Mn···Mn distance.

There is an inverse correlation between the Lewis acidity of the metals used for $Ca^{2+}$-replacement and the average Mn···Mn distance observed by EXAFS. The p$K_a$ values for the aquo ions are 8.10 ($Dy^{3+}$), 12.70 ($Ca^{2+}$), and 13.18 ($Sr^{2+}$).[67,68] Although these may be modified in the protein due to changes in coordination number[69] or ligation, the relative order of acidity should remain the same. The increase in Mn···Mn distance with increasing acidity of the metal in the $Ca^{2+}$ site raises the intriguing possibility that the variations in Mn···Mn distance may be due to changes in protonation state.

Previous work has shown that protonation of the $Mn_2(\mu\text{-}O)_2$ core in $[Mn^{IV}(salpn)(\mu\text{-}O)]_2$ causes the Mn···Mn distance to increase from 2.73 to 2.83 Å.[70] A second protonation causes a further 0.10-Å increase in Mn···Mn distance.[71] The changes that we observe following $Ca^{2+}$ substitution are significantly smaller and thus are not likely to represent complete protonation. If the observed changes in the average Mn···Mn distances are due to changes in only one of two $Mn_2(\mu\text{-}O)_2$ units,[72] then the actual change in Mn···Mn distance is −0.026 Å for $Sr^{2+}$ substitution and +0.030 Å for $Dy^{3+}$ substitution. One mechanism that could account for these changes is hydrogen bonding between a water bound to the $Ca^{2+}$ and a $Mn_2(\mu\text{-}O)_2$ unit (see

(64) The presence of 200 mM NaCl added to protect against Mn loss during the lanthanide incubation could potentially account for the change in Mn−Mn distance in the Dy-substituted sample. However, this is unlikely to be the case, since the $La^{3+}$-substituted sample and the $Dy^{3+}$-substituted sample have very different Mn···Mn distances, despite having the same $Cl^-$ concentration.

(65) Pettifer, R. F.; Hermes, C. *J. Appl. Crystallogr.* **1985**, *18*, 404−412.
(66) Pettifer, R. F. *Ital. Phys. Soc.* **1990**, *25*, 383−93.
(67) *IUPAC Dissociation constants of inorganic acids and bases in aqueous solution*; Perrin, D. D., Ed.; Butterworth and Co.: London, 1969.
(68) Huheey, J. E. *Inorganic Chemistry*, 3rd ed.; Harper and Row: New York, 1983.
(69) Evans, C. H. *Biochemistry of the Lanthanides*; Plenum Press: New York, 1990; Vol. 8, p 444.
(70) Larson, E. J.; Riggs, P. J.; Penner-Hahn, J. E.; Pecoraro, V. L. *J. Chem. Soc., Chem. Commun.* **1992**, 102−103.
(71) Baldwin, M. J.; Stemmler, T. L.; Riggs-Gelasco, P. J.; Kirk, M. L.; Penner-Hahn, J. E.; Pecoraro, V. L. *J. Am. Chem. Soc.* **1994**, *116*, 11349−11356.
(72) The present data provide no indication of whether one or both Mn−Mn distances are changed by Ca replacement. However, several studies (e.g., refs 39-41) have reported that perturbations of the OEC Mn cluster selectively affect one of two Mn−Mn distances at ca. 2.7 Å.

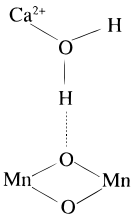


**Figure 10.** Proposed structural fragment of the OEC showing a hydrogen bond between a $Ca^{2+}$-bound water and a $Mn_2(\mu\text{-}O)_2$ unit. The remaining two Mn and the other ligands to both Mn and Ca are not shown.

Figure 10). When $Ca^{2+}$ is replaced with $Sr^{2+}$, the water will become less acidic and thus will form a weaker hydrogen bond to the oxo bridge. Conversely, when $Ca^{2+}$ is replaced with $Dy^{3+}$, the water will be more acidic and thus will form a stronger hydrogen bond. Since the Mn···Mn distance changes for both $Sr^{2+}$ and $Dy^{3+}$ replacements, this mechanism requires that the $Mn_2(\mu\text{-}O)_2$ oxo bridge have a p$K_a$ that is close to that of the water bound to the $Ca^{2+}$. It is impossible to predict the acidity of a water bound to the $Ca^{2+}$ without knowing the ligation environment of the $Ca^{2+}$ site. However, if we use the p$K_a$ of the aquo ion as a guide, Figure 10 suggests that the p$K_a$ of the $Mn_2(\mu\text{-}O)_2$ unit should be ca. 13. This is consistent with the p$K_a$ values that Pecoraro and co-workers have found for synthetic $Mn^{IV}_2(\mu\text{-}O)_2$ dimers.[73]

We emphasize that the structure in Figure 10 is highly speculative. In particular, we do not see any *direct* evidence for the Mn···Ca interaction. However, this scheme is consistent with many of the observations that have been made regarding the $Ca^{2+}$ site. It is known that modifications to the $Ca^{2+}$ site cause alterations in the EPR properties of the Mn cluster.[28,32,74] In Figure 10, this could be accomplished by changing the protonation of the $Mn_2(\mu\text{-}O)_2$ unit, since protonation of an oxo bridge has been shown to cause significant changes in the Mn···Mn magnetic coupling.[71] Removal of $Ca^{2+}$ has been reported to cause one of the Mn−Mn distances to increase from 2.7 to 3.0 Å, at least in the higher S states.[39] In Figure 10, this could be explained by loss of the oxo bridge that is hydrogen bonded to the $Ca^{2+}$ when the Ca is removed. It is known that the $Ca^{2+}$ is bound less tightly in the higher S states.[28] In Figure 10, this could be explained by the decrease in the acidity of the oxo bridge that is expected when the $Mn_2(\mu\text{-}O)_2$ unit is oxidized.[73] Lanthanide substitution prevents oxidation of Mn to form the $S_2$ state.[23] In Figure 10, this could be explained by the fact that lanthanide substitution will increase the protonation state of the $Mn_2(\mu\text{-}O)_2$ unit, thus increasing the reduction potential of the $Mn_2(\mu\text{-}O)_2$ core. In contrast, $Sr^{2+}$ substitution permits formation of an altered $S_2$ state. In Figure 10, this is consistent with the decreased Lewis acidity of $Sr^{2+}$. Finally, the small variations that we observe in the average Mn−O distance would also be consistent with Figure 10, since increased hydrogen bonding to the oxo bridge should result in a small increase in $Mn-O_{oxo}$ distances.

**Reconciliation with Previous Studies.** Our results differ from previous reports in two important ways. We find it impossible to distinguish between Mn and Ca or Sr by curve fitting alone, and we find no evidence for a change at ≈3.3 Å following Ca replacement. With regard to the former, we have demonstrated the difficulty in distinguishing scatterer identity at 3.3 Å using fit quality and amplitude functions alone. The fact that control samples can in some cases be fit equally well with Dy or Sr in place of Mn or Ca clearly illustrates this fact. This observation calls into question previous reports that Sr is required to fit the data in $Sr^{2+}$-substituted samples[43] and that Ca can be identified uniquely in control samples.[34] However, we have also demonstrated that it is possible to distinguish between Mn/Ca, Sr, and Dy based on phase differences. Based on the lack of change in the apparent Mn···M distance, it does not appear that Sr or Dy makes a significant contribution to the ≈3.3-Å feature in $Ca^{2+}$-replaced samples.

Yachandra et al. have reported that the substitution of $Sr^{2+}$ for $Ca^{2+}$ using a low pH citrate protocol results in a doubling of the amplitude of the 3.3-Å peak.[43] The samples used in the study by Yachandra et al. differ from those used here, since we have removed the 23- and 17-kDa extrinsic polypeptides, and since we did not use chelators for $Ca^{2+}$ removal. The extrinsic polypeptides could provide a binding site for $Ca^{2+}$ that is 3.3 Å from the Mn cluster. If so, we would not expect to observe any change at 3.3 Å in the absence of these polypeptides. Similarly, it is possible that chelator-induced structural changes are responsible for the differences between our results and those of Yachandra et al.,[43] since spectroscopic changes due solely to the presence of chelators have been noted. Ono et al. attributed some of the changes observed with the citrate−$Ca^{2+}$ removal protocol to irreversible structural modification of the Mn cluster by citrate.[60] Boussac et al. noted that high concentrations of EGTA (10 mM) cause modification of the multiline signal relative to that seen for samples having only low concentrations of EGTA (50 $\mu$M), even though both samples were subjected to the same calcium removal protocol prior to incubation in EGTA.[32] Furthermore, these changes were similar to those induced by incubation in 40 mM citrate at pH 6.5, a condition where $Ca^{2+}$ is not removed. The changes caused by pH 6.5 incubation in citrate were not induced with acetate, and appear to require the presence of polycarboxylic acids. The binding of citrate to the Mn cluster could change the carbon density and thus the EXAFS amplitude at ≈3.3 Å. Alternatively, the binding of carboxylates to a Mn/Ca pair that is normally not EXAFS detectable could make the Mn/Ca interaction more rigid and thus EXAFS detectable.

However, it appears unlikely that the absence of either the extrinsic polypeptides or chelators is responsible for our results, given the similarity in the EPR spectra for our $Sr^{2+}$-substituted sample and other $Sr^{2+}$-substituted samples. Moreover, recent EXAFS measurements comparing structural parameters obtained for BBY type preparations, which contain the 17- and 23-kDa polypeptides, with detergent core complexes similar to those used in this study, did not find any significant changes between the two types of preparations.[34] This again suggests that the differences between our results and those of Yachandra et al. are not due to differences in samples.

## Conclusions

The low-temperature EXAFS spectra for the OEC contain a shell of Mn···M scatterers at ca. 3.3 Å. The change of M from Ca to Sr or Dy would not be expected to result in major changes in the EXAFS amplitude, but should result in detectable changes in the apparent Mn···M distance at ca. 3.3 Å. The absence of any change in the ca. 3.3 Å Mn···M distance when $Ca^{2+}$ is replaced by $Sr^{2+}$ or $Dy^{3+}$ suggests that there are no EXAFS detectable Mn···Ca interactions at 3.3 Å in our samples. Instead, the third peak in the Fourier transform is attributed to Mn···Mn, and possibly Mn···C, EXAFS. Although there are no significant changes in this feature when Ca is replaced, there are nevertheless small changes in the Mn core structure that

(73) Baldwin, M. J.; Gelasco, A.; Pecoraro, V. L. *Photosynth. Res.* **1993**, *38*, 303−308.

(74) Boussac, A.; Zimmerman, J.-L.; Rutherford, A. W. In *Current Research in Photosynthesis*; Baltscheffsky, M., Ed.; Kluwer Academic Publishers: The Netherlands, 1990; Vol. 1, pp 713−716.

occur as a result of $Ca^{2+}$ substitution. One model which can account for the change in Mn···Mn distance involves hydrogen bonding between a $Ca^{2+}$-bound water and a $Mn_2(\mu\text{-}O)_2$ unit. If correct, this scheme would suggest that a crucial role for the $Ca^{2+}$ in the OEC may be to modulate the protonation state, and thus the reduction potential, of the Mn cluster. This model, while speculative, is consistent with the known effects of Ca replacement. Experiments are in progress to test the validity of this structural model.

**Acknowledgment.** This research is supported in part by Grant No. USDA-NRICGP-92-37306-7662 to C.F.Y. and Grant No. GM-45205 from the US National Institute of Health to J.P.H. P.J.R.G. was supported in part by an NIH research traineeship. S.S.R.L. and N.S.L.S. are supported by the US Department of Energy with additional support from the NIH Research Resource program. We wish to thank Dr. Vincent Pecoraro and Dr. Erlund Larson for supplying the compound $[Mn^{III}(salpn)(OCH_3)]_2$ for comparison to protein data.

**Note Added in Proof:** While this paper was being reviewed, Klein and co-workers reported a similar study of $Sr^{2+}$ substituted samples.[75] They found changes in fit quality and distance for Sr vs Ca that are similar to those that we see. They interpret these as evidence for a Mn−Ca interaction at ca. 3.4−3.5 Å.

**Supporting Information Available:** Best 3 shell fits to filtered data (O, Mn, Mn and O, Mn, Dy) for a control $S_1$ sample (Figure S1) and corresponding $Dy^{3+}$-substituted sample (Figure S2) (2 pages). This material is contained in many libraries on microfiche, immediately follows this article in the microfilm version of the journal, can be ordered from the ACS, and can be downloaded from the Internet; see any current masthead page for ordering information and Internet access information.

JA9504505

(75) Latimer, M. J.; DeRose, V. J.; Mukerji, I.; Yachandro, V. K.; Sauer, K.; Klein, M. P. *Biochemistry* **1995**, *34*, 10898−10909.